

CHAOS IN A DISK GALAXY MODEL INDUCED BY ASYMMETRIES IN THE DARK HALO

N. D. Caranicolas and E. E. Zotos

*Department of Physics, Section of Astrophysics,
Astronomy and Mechanics, Aristotle University of Thessaloniki,
541 24 Thessaloniki, Greece; caranic@astro.auth.gr*

Received: 2009 June 10; accepted: 2009 September 22

Abstract. We study the regular or chaotic nature of motion in a disk galaxy with a dense nucleus and an asymmetric dark halo. Two cases, the 2D model and the 3D model, are investigated. In the 2D model, a considerable fraction of the phase plane is covered by chaotic orbits. Two factors seem to be responsible for the chaotic motion: (i) the dense nucleus and (ii) the asymmetries in the dark halo. Our numerical experiments suggest, that there are several chaotic components on the Poincaré phase plane. Different chaotic components are induced by the asymmetries in the halo. Each chaotic component seems to have a different value of the Lyapunov Characteristic Exponent, for small values of the asymmetry parameter λ and a unique LCE for larger values of λ . A comparison of the present results with outcomes from previous work is also presented.

Key words: galaxies: kinematics and dynamics – galaxies: star orbits: regular and chaotic motion, halos

1. INTRODUCTION

Galaxies are often surrounded by halos. In most cases the shape of halo is spherical or nearly spherical but there are also indications that the shape of halo may be a biaxial or even a triaxial ellipsoid (see Kunihito et al. 2000; Olling & Merrifield 2000; Wechsler et al. 2002; Caranicolas & Zotos 2009). The distinction between the halo and the main body of the galaxy is clearest in disk galaxies, where the spherical or the triaxial shape of the halo contrasts with the flat disc. In an elliptical galaxy, there is no sharp transition between the body of the galaxy and the halo. The visible part of the halo, is occupied by population II objects, including globular clusters and old individual stars. Beyond this, is a much larger region, called the dark halo or extended halo, containing large amounts of dark matter. Note that the stellar halo is not an inner part of the dark halo. They are two physically distinct components with different formation histories. We would like to point out that the above mentioned triaxial dark halo models are all symmetrical, unlike the dark halo model in the present paper.

The need for existence of dark halos results from many independent sources

such as rotation curves, hot gas in clusters, velocity dispersions of galactic groups, gravitational lensing and microwave radiation. The presence of dark matter in the halo is demonstrated by its gravitational effect on the rotation curve of the disk. Without large amounts of mass in the extended halo, the rotational velocity of the galaxy should decrease at large distance from the galactic core. However, observations of disk galaxies, particularly radio observations of line emission from neutral atomic hydrogen, show that the rotation curve of most spiral galaxies remains flat far beyond the visible matter. The absence of any visible matter to account for these observations implies the presence of unobserved matter. The nature of dark matter in the galactic halo of spiral galaxies is still undetermined, but the most popular theories accept that the dark halo is populated by vast numbers of small bodies known as MACHOs. Observations of the halo of the Milky Way show that the number of MACHOs is not likely to be sufficient to account for the required mass.

No doubt that the behavior of orbits in the galactic disk is affected by the presence of the halo. Of particular interest is to study the effect of the asymmetries of the dark halo in the behavior of orbits in the disk. In order to investigate this behavior we have constructed a composite 3D dynamical model of a disk galaxy. The model is described in Section 2. In Section 3 we use the $x - p_x$ phase plane in order to study the motion in the 2D model. In Section 4 we use the results obtained from the 2D model in order to visualize the motion in the 3D model. Of special interest is to find the behavior of 3D orbits in different chaotic components observed in the 2D model. We close our research with discussion and conclusions which are presented in Section 5.

2. PRESENTATION OF THE DYNAMICAL MODEL

Our model consists of three distinct components – the disk halo, the nucleus and the dark halo component. The disk halo component is described by the potential

$$V_d(x, y, z) = \frac{-M_d}{\sqrt{b^2 + x^2 + y^2 + (a + \sqrt{h^2 + z^2})^2}}, \quad (1)$$

where M_d is the mass, b is the core radius of the disk halo, α is the disk scale length and h is the disk scale height. Potential (1) was introduced by Miyamoto & Nagai (1975). The dense massive nucleus is described by the spherical potential

$$V_n(x, y, z) = \frac{-M_n}{\sqrt{x^2 + y^2 + z^2 + c_n^2}}, \quad (2)$$

where M_n is the mass and c_n is the scale length of the nucleus. For the dark halo we use the logarithmic potential

$$V_h(x, y, z) = \frac{v_0^2}{2} \ln[x^2 + y^2 + z^2 - \lambda x^3 + c_h^2]. \quad (3)$$

Here c_h is the scale length of the dark halo component and the parameter v_0 is used for the consistency of the galactic units. The term $-\lambda x^3$, $\lambda \ll 1$ represents the deviation of the halo from spherical symmetry (see also Binney & Tremaine 2008).

We use the system of galactic units, where the unit of length is 1 kpc, the unit of mass is $2.325 \times 10^7 M_\odot$ and the unit of time is 0.97748×10^8 yr. The velocity unit is 10 km/s, while G is equal to unity. The energy unit (per unit mass) is $100 (\text{km/s})^2$. In the above units we use the values: $v_0 = 20, \alpha = 3, b = 6, h = 0.325, M_d = 12000$. The value of c_n and c_h is 0.25 and 8 respectively while M_n and λ are treated as parameters.

The total potential responsible for the motion of a test particle of unit mass in the galaxy is

$$V_T(x, y, z) = V_d + V_n + V_h. \quad (4)$$

There are three lines of arguments to justify the choice of potential (4). The first is that the disk nucleus potential system given by equations (1) and (2) is a classical realistic potential, which describes very well the motion in an active disk galaxy. The second is that potential (3) describes satisfactorily the deviation of the dark halo from spherical symmetry, and the third is that there is observational evidence that asymmetries in the halos do exist (see Xu et al. 2007). However we must emphasize that (Xu et al. 2007) investigated the stellar halos, not the dark halos.

The equations of motion are:

$$\ddot{x} = -\frac{\partial V_T}{\partial x}, \ddot{y} = -\frac{\partial V_T}{\partial y}, \ddot{z} = -\frac{\partial V_T}{\partial z}, \quad (5)$$

where the dot indicates derivative with respect to the time. The corresponding Hamiltonian is

$$H = \frac{1}{2}(p_x^2 + p_y^2 + p_z^2) + V_T(x, y, z) = E, \quad (6)$$

where p_x, p_y, p_z are the momenta per unit mass, conjugate to x, y and z while E is the numerical value of the Hamiltonian.

3. NUMERICAL RESULTS FOR THE 2D MODEL

In this case we integrate numerically the equations of motion (5) with $z = p_z = 0$. The corresponding Hamiltonian is

$$H_2 = \frac{1}{2}(p_x^2 + p_y^2) + V_T(x, y) = h_2, \quad (7)$$

where h_2 is the numerical value of the energy of the test particle.

We believe that it is a good idea to start from the 2D system for two basic reasons: (i) in the 2D system we can use the $x - p_x, y = 0, p_y > 0$ Poincaré phase plane in order to locate the areas of regular and chaotic motion, and (ii) we can use the experience gained from the study of the 2D system in order to explore a more complicated 3D system.

Figure 1 shows the $x - p_x$ phase plane when $\lambda = 0.015, M_n = 400, h_2 = 500$. We see that the larger part of the phase plane is covered by regular orbits. There are also parts of the phase plane occupied by chaotic orbits. Three distinct areas of chaotic motion are observed: a considerable chaotic layer near the central region and two secondary chaotic components which appear near the unstable periodic orbit produced by secondary resonances. Figure 2 is similar to Figure 1 but for $h_2 = 300$. Here one can see only the chaotic layer near the central part of the

phase plane while no other chaotic component seems to be present. The rest of the phase plane is covered by regular orbits. Thus we may conclude that, as a result, the asymmetry in the dark halo has to produce a different chaotic component for the high energy stars. In other words, the asymmetry affects not only stars approaching the dense nucleus but also stars moving far from the nuclear region. On the other hand, from the totality of low energy stars only those approaching the nucleus are on chaotic orbits.

Figure 3 is similar to Figure 1 but for $\lambda = 0.03$. In Figure 3 we see that the three chaotic components have merge to produce a large chaotic sea, while the small regular regions are confined near the stable resonant periodic points. Furthermore, in Figure 4 we see that the picture is almost the same as that shown in Figure 2. The only difference is that here one can observe some additional small islands produced by secondary resonances. Thus, one can see that the increase of the asymmetry in the halo affects drastically the high energy stars, producing large chaotic regions by merging different chaotic components. Moreover, low energy stars seem to display only one chaotic layer, which is produced by low energy stars approaching the dense nucleus.

Figures 5(a–d) show four typical orbits for the 2D potential. The values of the parameters are as in Figure 1. Panel (a) shows a quasi periodic orbit. The initial conditions are: $x_0 = -6.5, y_0 = 0, p_{x0} = 19, h_2 = 500$. The value of p_y is always found from energy integral (7). Panel (b) shows a tube orbit with the initial conditions $x_0 = 7.0, y_0 = 0, p_{x0} = 0$ and $h_2 = 300$. A quasi periodic orbit is also presented in panel (c). The initial conditions are: $x_0 = -3.0, y_0 = p_{x0} = 0$ and $h_2 = 300$. Note that all the above quasi periodic orbits do not approach the dense nucleus. Panel (d) shows a chaotic orbit with the initial conditions $x_0 = 0.5, y_0 = p_{x0} = 0$ and $h_2 = 500$. This orbit comes arbitrary close to the nucleus. The orbits were calculated for a time period of 100 time units.

It would be of particular interest to follow the evolution of chaotic regions, as the parameter λ increases or as the mass of the nucleus M_n increases, when all other parameters are kept constant. The results are presented in Figures 6 and 7. Figure 6 shows a plot of the percentage of the surface of section $A\%$ covered by chaotic orbits vs. λ , when $M_n = 400$. The values of all other parameters are as in Figure 1. Dots indicate the values found numerically, while the solid line is a two degree polynomial fit. We see that $A\%$ increases rapidly as λ increases. Figure 7 shows a plot of $A\%$ vs. M_n , when $\lambda = 0.015$. The values of all other parameters are as in Figure 1. Again, dots indicate the values found numerically, while the solid line is a two degree polynomial fit. Here we see that $A\%$ increases as M_n increases but at a smaller rate.

It is also of interest to compute the Lyapunov Characteristic Exponents (LCE) (see Lichtenberg & Lieberman 1992) in order to estimate the degree of chaos in different chaotic regions of Figure 1, i.e., when $\lambda = 0.015, M_n = 400, h_2 = 500$. The LCE in all cases was computed for a time period of 20000 time units. Note that this time period is at least 100 times larger than the corresponding Hubble time. The LCE was found to be 0.195 in the chaotic region near the center. The value of the LCE on the left and right chaotic components was found to be 0.020 and 0.010, respectively. As expected, each chaotic component has a different LCE. This phenomenon was observed in disk galaxies without a halo component (see Fig. 3 in Papadopoulos & Caranicolas 2005). It was also observed in potentials made up of perturbed harmonic oscillators (see Saito and Ichimura

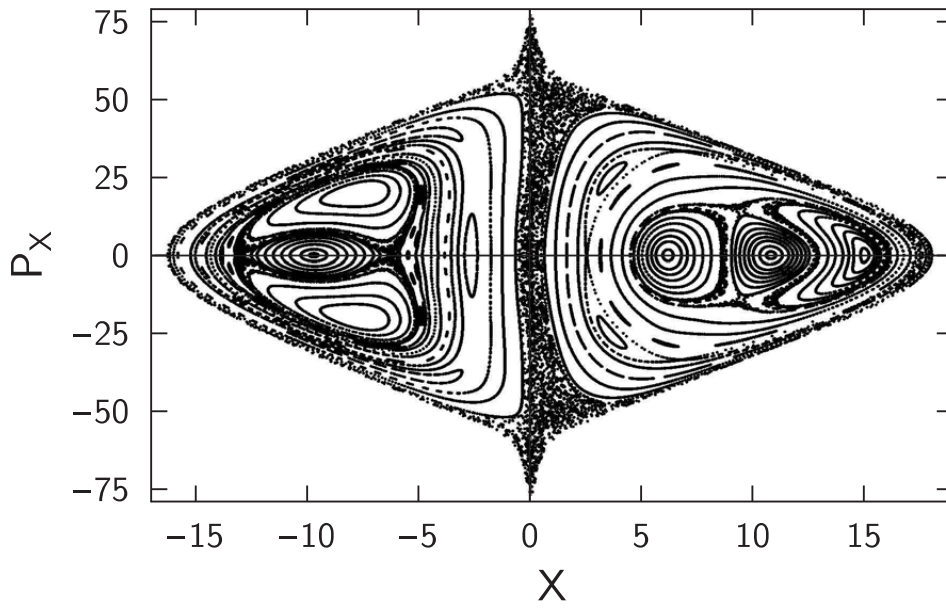


Fig. 1. The $x - p_x$ phase plane of the 2D system. The values of the parameters are: $v_0 = 20, \alpha = 3, b = 6, h = 0.325, M_d = 12000, c_n = 0.25, c_h = 8, M_n = 400, \lambda = 0.015$ and $h_2 = 500$.

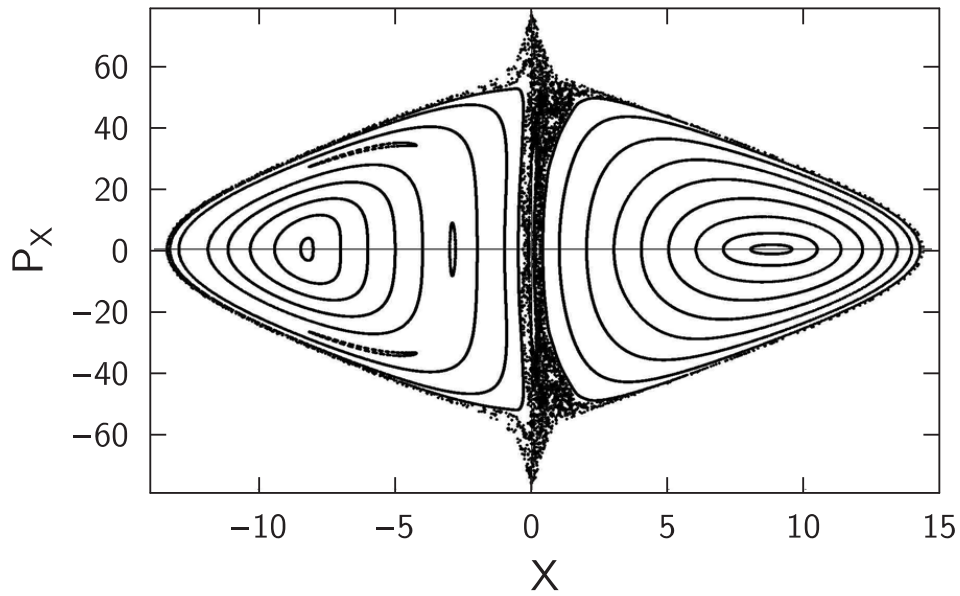


Fig. 2. The same as in Figure 1 but for $h_2 = 300$.

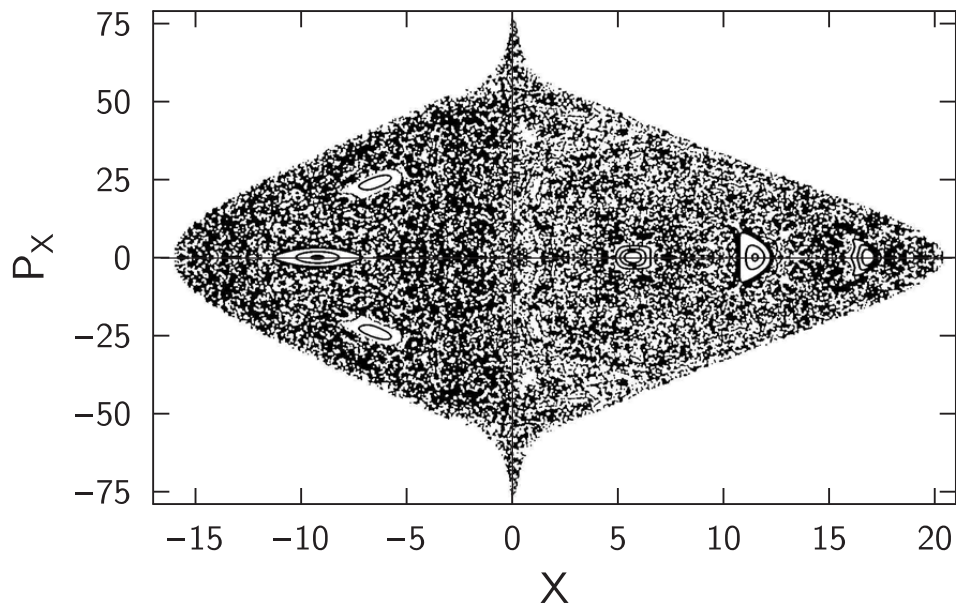


Fig. 3. The $x - p_x$ phase plane of the 2D system. The values of the parameters are: $v_0 = 20$, $\alpha = 3$, $b = 6$, $h = 0.325$, $M_d = 12000$, $c_n = 0.25$, $c_h = 8$, $M_n = 400$, $\lambda = 0.03$ and $h_2 = 500$.

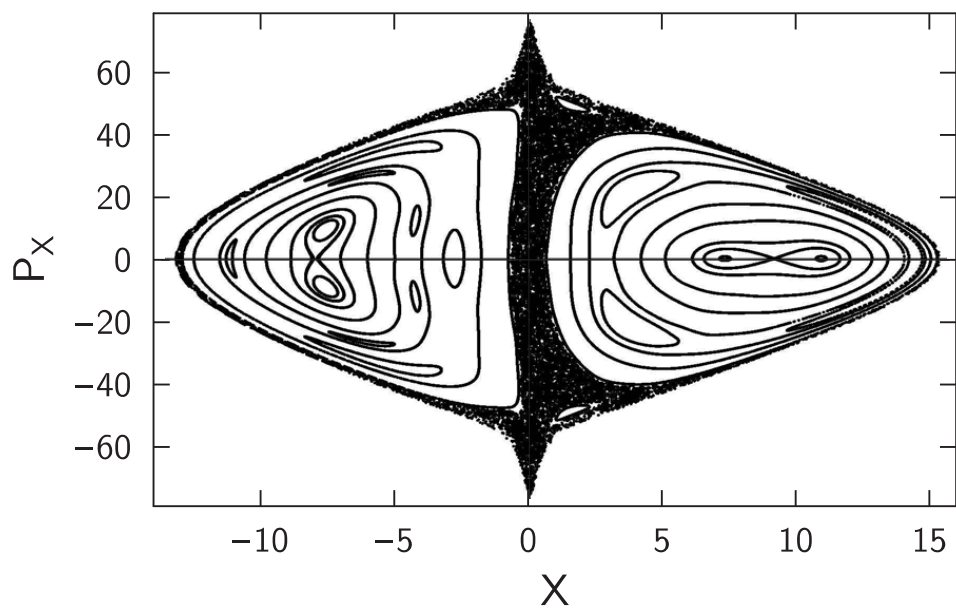


Fig. 4. The same as in Figure 3 but for $h_2 = 300$.

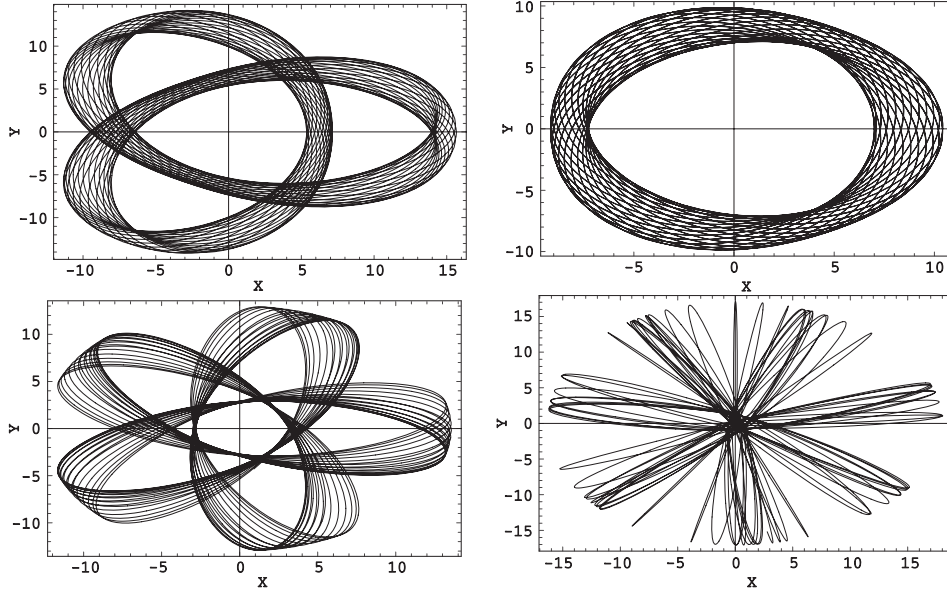


Fig. 5. Panels (a)–(d): typical orbits for the 2D potential. The values of the parameters are as in Figure 1. Panel (a) – upper left: a quasi-periodic orbit with the initial conditions: $x_0 = -6.5$, $y_0 = 0$, $p_{x0} = 19$ and $h_2 = 500$. Panel (b) – upper right: a tube orbit with the initial conditions: $x_0 = 7.0$, $y_0 = 0$, $p_{x0} = 0$ and $h_2 = 300$. Panel (c) – lower left: a quasi periodic orbit with the initial conditions $x_0 = -3.0$, $y_0 = 0$, $p_{x0} = 0$ and $h_2 = 300$. Panel (d) – lower right: a chaotic orbit with the initial conditions $x_0 = 0.5$, $y_0 = 0$, $p_{x0} = 0$ and $h_2 = 500$. The value of p_y is always found from the energy integral.

1978). Moreover, the LCE for all orbits, starting in the chaotic sea of Figure 3, i.e., when $\lambda = 0.03$, $M_n = 400$, $h_2 = 500$, was found to be 0.165. This result is not surprising as in Figure 3 different chaotic regions have merged.

4. ORBITS IN THE 3D MODEL

Let us now turn to the properties of orbits in the 3D potential. In order to do this, we compute orbits with initial conditions (x_0, p_{x0}, z_0) , $y_0 = p_{y0} = 0$, where (x_0, p_{x0}) is a point inside the limiting curve of the 2D system. The limiting curve corresponds to

$$\frac{1}{2}p_x^2 + V_T(x) = h_2 \quad (8)$$

and can be obtained from (7) if we set $y = p_y = 0$. For convenience, we take $E = h_2$ and the value of p_{y0} is always found from the energy integral (6).

Our numerical calculations suggest that all orbits in the 3D model, starting with initial conditions (x_0, p_{x0}) on the chaotic zones of the 2D system of Figure 1, i.e., when $\lambda = 0.015$, $M_n = 400$, $E = h_2 = 500$, and all permissible values of z_0 , i.e. such as to obtain real values for p_y , are chaotic. The values of the LCE are different for the 3D orbits starting in different chaotic zones. Thus, the value of the LCE for orbits starting with (x_0, p_{x0}) in the chaotic zone near the center was found to be 0.105. For the chaotic zone on the left-hand side of Figure 1, the LCE

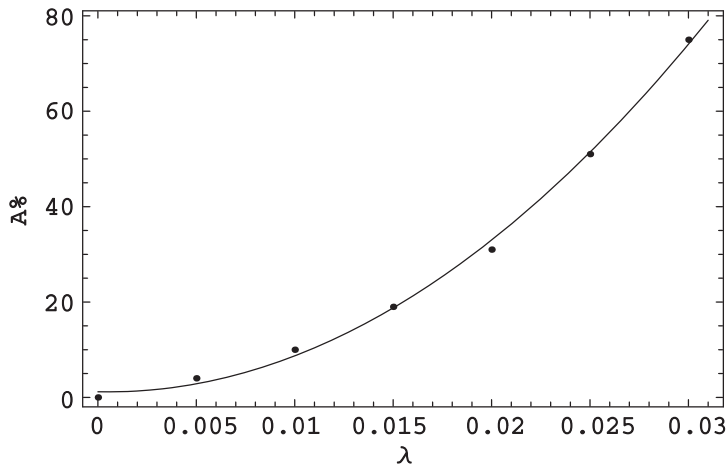


Fig. 6. A plot of the percentage of the surface of section $A\%$ covered by chaotic orbits vs. λ , when $M_n = 400$.

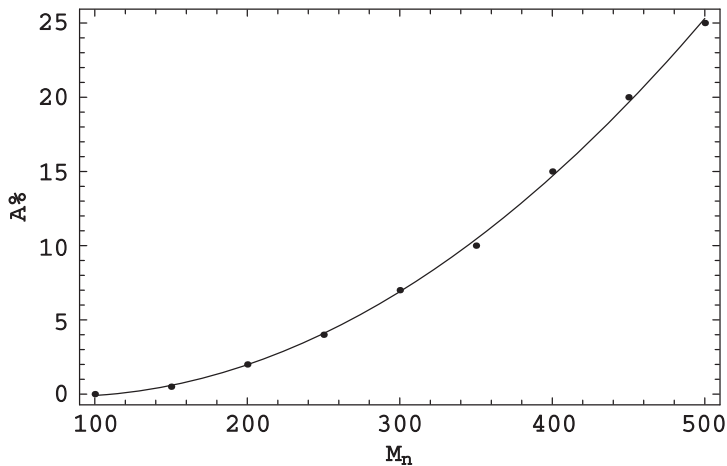


Fig. 7. A plot of the percentage of the surface of section $A\%$ covered by chaotic orbits vs. M_n , when $\lambda = 0.015$.

was found to be 0.015 while for the chaotic zone on the right-hand side of Figure 1 it was 0.008. These results seem to be correct because there is no evidence yet that in 3D systems with divided phase space a completely connected chaotic component actually exists (see Cincotta et al. 2006). On the other hand, all orbits with initial conditions (x_0, p_{x0}, z_0) , $y_0 = p_{z0} = 0$, with values of (x_0, p_{x0}) in the chaotic sea of Figure 3, were found chaotic for all permissible values of z_0 . The corresponding LCE was found to converge to a common value, equal to 0.124.

In order to have a complete picture of the behavior of orbits in the 3D system, we have calculated a large number of orbits with initial conditions, (x_0, p_{x0}, z_0) , $y_0 = p_{z0} = 0$ with the values of (x_0, p_{x0}) in the regular regions of Figure 1. It was found that for the values $|z_0| < 4$ all tested orbits were found regular, while when $|z_0| \geq 4$ the orbits were found chaotic. The value of the LCE was found to be

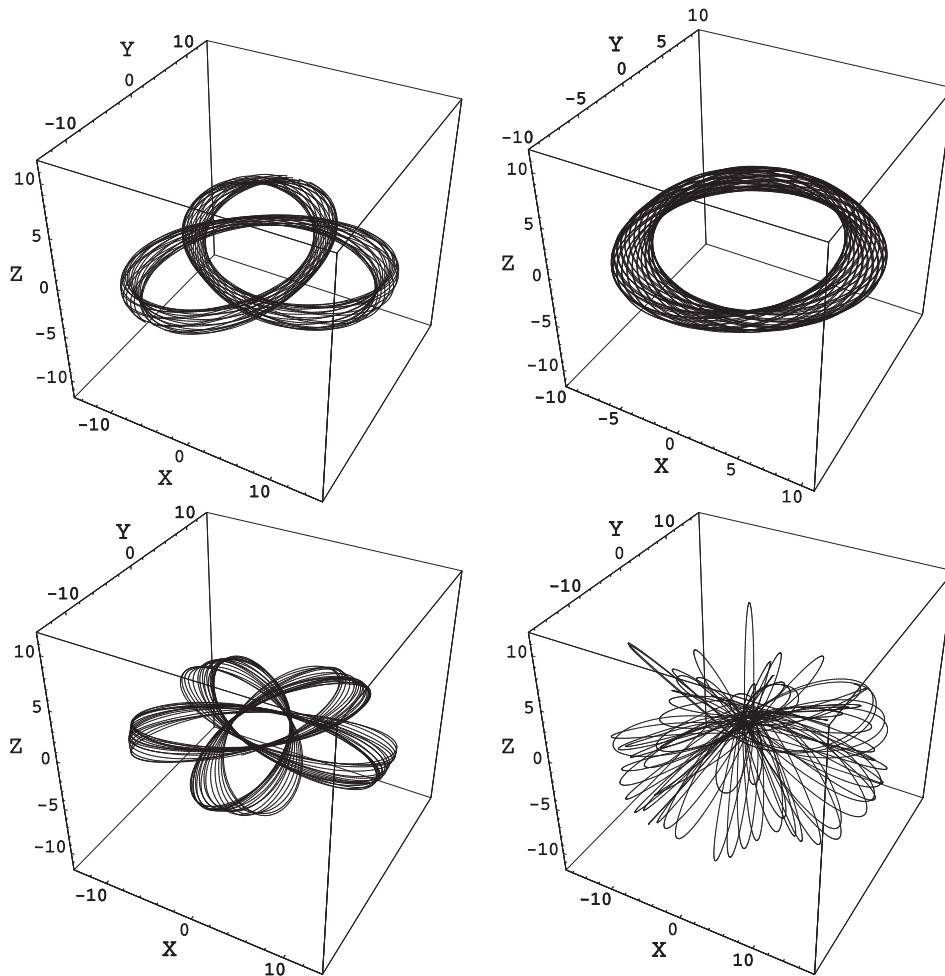


Fig. 8. Panels (a)–(d): representative orbits in the 3D potential. Initial conditions for x_0, p_{x0} as in Figures 5a–5d, respectively, while $z_0 = 0.1$ and $E = h_2$ for all orbits. Note that the chaotic orbit in Figure 5d is scattered to the halo.

between 0.005–0.008 for orbits starting on the left-hand side of Figure 1, while for orbits on the right-hand side of Figure 1 the LCE takes values in a range of 0.010–0.015.

Figures 8 (a–d) show four representative orbits in the 3D potential. In order to better visualize the behavior of the 3D orbits, we have used the same initial conditions of the orbits as in Figures 5 (a–d) for the 2D system, with the same value of energy, $E = h_2$. The value of z_0 was taken to be equal to 0.1 for all orbits. It is seen that all orbits retain their regular or chaotic character. Furthermore, one can see only chaotic orbits approach the dense nucleus while regular orbits do not. All orbits were calculated for a time period of 100 time units.

It is also interesting to note that, from all the above four orbits starting near the galactic plane, only that approaching the nucleus is deflected to the halo. There-

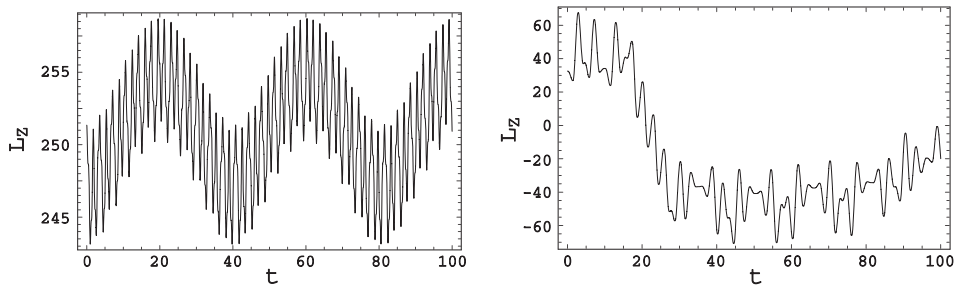


Fig. 9. Evolution of the angular momentum vs. time: the left panel is for the quasi-periodic orbit of Figure 8b and the right panel is for the chaotic orbit of Figure 8d.

fore, we can say that orbits moving near the galactic plane, when approaching the dense nucleus, are scattered to higher z . This behavior is similar to that observed about twenty years ago by Caranicolas & Inannen (1991) in axially symmetrical disk galaxies, hosting dense nuclei. Today it is well known that for this scattering is responsible the strong F_z nuclear force, that acts upon the low angular momentum stars (see also Caranicolas & Papadopoulos 2003).

We would also like to remind the reader that, in any case, the orbits that are scattered to the halo are orbits of low angular momentum. As here the L_z component of the angular momentum is not conserved, we can compute its mean value

$$\langle L_z \rangle = \frac{1}{n} \sum_{k=1}^n L_{zk}. \quad (9)$$

Figure 9a shows the evolution of angular momentum vs. time for the orbit shown in Figure 8b. As expected, one can observe a quasi periodic curve while $\langle L_z \rangle = 251$. Figure 9b is similar to Figure 9a but for the chaotic orbit of Figure 8d. Here one can see an asymmetric curve and $\langle L_z \rangle = -27.1$. Both orbits were calculated for a time period of 100 time units and with $n = 10^4$.

5. DISCUSSION

It is well known that the evolution of galaxies is closely associated to the shape and the structure of the host halos. Today astronomers believe that dark halos may have a variety of shapes and they usually show asymmetries (see, e.g., Dinshaw et al. 1998; Oppenheimer et al. 2001; McLin et al. 2002; Penton et al. 2002; Steidel et al. 2002).

In the present paper, the behavior of orbits in a galaxy with an asymmetric dark halo component was investigated. In order to keep things simple, we have chosen a nearly spherical dark halo component with a small deviation from spherical symmetry, introduced by the term $-\lambda x^3$. The results of this work strongly suggest, that small asymmetries in the halo may play an important role on the regular or chaotic nature of orbits.

We have first studied the 2D system using the classical method of the Poincaré phase plane. Our numerical experiments show that there are three distinct areas of chaotic motion when $\lambda = 0.015$ and $h_2 = 500$: a chaotic layer in the central region and two additional chaotic regions, which appear near the unstable periodic orbits produced by the secondary resonances. As expected, the LCE was found

to be different in each chaotic region. On the other hand, when $\lambda = 0.03$ and $h_2 = 500$, the LCE was found to converge to a unique value when the three chaotic regions merge to form a large chaotic sea.

Using the results of the 2D system, we have investigated the 3D potential. We have used initial conditions (x_0, p_{x0}, z_0) , where (x_0, p_{x0}) was a point on the phase plane. It was found, that all orbits starting in the chaotic regions on the phase plane, produce chaotic orbits for all values of z_0 . Note that in all cases the value of p_y was found from the energy integral, while $y = p_z = 0$. Our numerical results indicate that the three chaotic components, found in the 2D system, exist also in the 3D potential and have also different values of the LCE when $\lambda = 0.015$. Furthermore, when $\lambda = 0.03$ and the three chaotic components merge, as it was indicated in the phase plane of the 2D system, the LCE of the 3D system seems to converge to a unique value. This result is in agreement with the outcomes for the 3D systems obtained by Cincotta et al. (2006).

It was also found that orbits starting in the regular parts of the 2D system display chaotic motion only when $|z_0| \geq 4$. Orbits with low values of $\langle L_z \rangle$, moving near the galactic plane, when approaching the dense and massive nucleus, are scattered to the halo displaying chaotic motion. This behavior was also observed in axially symmetrical disk galaxies with dense massive nuclei (see also Caranicolas & Papadopoulos 2003 and references therein). Thus, one can conclude that low angular momentum stars are on chaotic orbits in axially symmetrical, as well as in triaxial galaxies, hosting massive and dense nuclei.

ACKNOWLEDGMENT. The authors would like to thank the referee Peeter Tenjes for his useful suggestions and comments.

REFERENCES

- Binney J., Tremaine S. 2008, *Galactic Dynamics*, Princeton Series in Astrophysics, 2nd edition
- Caranicolas N. D., Innanen K. A. 1991, *AJ*, 102, 1343
- Caranicolas N. D., Papadopoulos N. 2003, *A&A*, 399, 957
- Caranicolas N. D., Zotos E. E. 2009, *Astron. Nachr.*, in press
- Cincotta P. M., Giordano C. M. et al. 2006, *A&A*, 455, 499
- Dinshaw N., Foltz C. B. et al. 1998, *ApJ*, 494, 567
- Kunihito I., Takahiro T. et al. 2000, *ApJ*, 528, 51
- Lichtenberg A. J., Leiberman M. A. 1992, *Regular and Chaotic Dynamics*, Springer, 2nd edition
- Miyamoto M., Nagai R. 1975, *PASJ*, 27, 253
- McLin K., Stocke J. T. et al. 2002, *ApJ*, 574, L115
- Olling R. P., Merrifield M. R. 2000, *MNRAS*, 311, 361
- Oppenheimer N. C., Hambly A. P. 2001, *Science*, 292, 698
- Papadopoulos N., Caranicolas N. D. 2005, *Baltic Astronomy*, 14, 253
- Penton S. V., Stocke J. T., Shull J. M. 2002, *ApJ*, 565, 720
- Saito N., Ichimura A. 1979, in *Stochastic Behavior in Classical and Quantum Hamiltonian Systems*, Eds. G. Casati & J. Ford, Springer, p. 137
- Steidel C. C., Kollmeier J. A. et al. 2002, *ApJ*, 570, 526
- Xu Y., Deng L. C., Hu J. Y. 2007, *MNRAS*, 379, 1373
- Wechsler R. H., Bullock J. et al. 2002, *ApJ*, 568, 52